

Scaling of Dirac fermions and the WKB approximationJ. W. Van Orden,^{1,2} Sabine Jeschonnek,³ and John Tjon^{4,5}¹*Department of Physics, Old Dominion University, Norfolk, Virginia 23529, USA*²*Jefferson Lab, 12000 Jefferson Ave, Newport News, Virginia 23606, USA*³*The Ohio State University, Physics Department, Lima, Ohio 45804, USA*⁴*Department of Physics, National Taiwan University, Taipei 10617, Taiwan*⁵*KVI, University of Groningen, The Netherlands*

(Received 25 July 2005; published 23 September 2005)

We discuss a new method for obtaining the WKB approximation to the Dirac equation with a scalar potential and a timelike vector potential. We use the WKB solutions to investigate the scaling behavior of a confining model for quark-hadron duality. In this model, a light quark is bound to a heavy diquark by a linear scalar potential. Absorption of virtual photons promotes the quark to bound states. The analog of the parton model for this case is for a virtual photon to eject the bound, ground-state quark directly into free continuum states. We compare the scaling limits of the response functions for these two transitions.

DOI: [10.1103/PhysRevD.72.054020](https://doi.org/10.1103/PhysRevD.72.054020)

PACS numbers: 12.40.Nn, 12.39.Ki, 13.60.Hb

I. INTRODUCTION

Quark-hadron duality implies that, in certain kinematic regimes, properly averaged hadronic observables can be described by a perturbative QCD (pQCD) calculation. This version of duality is highly relevant as perturbative QCD calculations can be performed. Using duality, these pQCD calculations can then be related to averaged data taken in the resonance region. Duality was first observed more than 30 years ago experimentally by Bloom and Gilman in inclusive inelastic electron scattering [1], and has since then been observed in a variety of reactions: $e^+e^- \rightarrow$ hadrons is an example for duality we know from the textbooks; the semileptonic decay of heavy mesons is another example [2–4]. Duality is considered in the analysis of heavy ion reactions [5], and forms the basis for using QCD sum rules [6]. Recently, duality has been observed to high precision and down to rather low momentum transfers in electron scattering at Jefferson Lab [7–10]. Duality in spin observables is currently probed by several experiments, both at Jefferson Lab and at DESY in Germany [11–14]. In addition to the “classical” examples and applications of duality, duality ideas are applied in new areas, too. For neutrino scattering, the beam energies are not well known, and an averaging will thus take place almost automatically. The application of duality is discussed for several planned neutrino experiments, see e.g. [15], and duality ideas have been applied in [16] to nucleon/nuclear duality in neutrino scattering. There is also interest in duality in parity violation experiments [17], and with regard to generalized parton distributions [18,19]. A very local version of duality—assuming that it holds for just one resonance—has been used in [20,21] to extract information on structure functions at $x_{Bj} \rightarrow 1$ in the scaling limit from form factor data. These ideas were also applied to neutrino-nucleon scattering [21]. Duality ideas might also be useful for pion photoproduction [22]. Duality is a major point in the

12 GeV upgrade of CEBAF at Jefferson Lab [23]. A recent review of quark-hadron duality can be found in [24].

Apart from being interesting all by itself, quark-hadron duality is an important tool for studying kinematic areas that cannot be accessed in the deep inelastic regime: measurements at large values of x_{Bj} in the resonance region typically have much higher count rates than measurements at the same x_{Bj} in the deep inelastic regime, which requires very high four-momentum transfers Q^2 . Application of a proper averaging procedure to the resonance data may allow the extraction of deep inelastic information, e.g. in the case of the polarization asymmetry A_1 of the neutron for $x_{Bj} \rightarrow 1$. Before duality averaging procedures can be applied safely, we require a thorough understanding of where duality holds and how exact it is. Therefore, duality has been studied intensively by theorists during the past couple of years [18,20,21,25–49]. Most of the theoretical studies focus on duality in electron scattering, due to the large experimental program. The model we will discuss here is for electron scattering, too.

Many recent papers have been devoted to modeling quark-hadron duality in simple, fully solvable relativistic models, to gain a better understanding of the conditions under which duality works [18,27,33–35,40–43]. The idea of modeling duality is to capture just the essential physical conditions of this rather complex phenomenon. Typically, these basic requirements for a model are imposed: one requires a relativistic description of confined valence quarks, and one treats the hadrons in the infinitely narrow resonance approximation.

In these papers, one important point was raised and discussed that is interesting not just for duality, but in general: do the scaling curves obtained assuming outgoing plane waves agree with the scaling curves obtained when we assume final state interactions?

The general approach is to model the pQCD picture by considering a quark bound within a potential in the initial

state, and after the interaction with a virtual photon, the quark is considered “free” and the potential set to zero. This “bound-free” transition corresponds to a plane-wave impulse approximation (PWIA). This transition is compared with a hadronic picture: the initial state is the same—the quark is bound in a potential—but after the absorption of the photon, it is in an excited, but still bound, state. This “bound-bound” transition corresponds to the excitation of resonances.

In order to reproduce duality, a model must fulfill several conditions that are observed experimentally: first, the bound-free transition, corresponding to pQCD, must scale for large momentum transfers. Second, the bound-bound transition must scale, and the bound-bound and bound-free scaling functions have to agree so that the third condition can be fulfilled: at low momentum transfers, the bound-bound results should oscillate around the bound-free scaling curve. Note that in all models currently proposed, there are no gluons included, and therefore neither radiative corrections nor evolution of scaling curves are present.

In our recent papers [40,41], we could show analytically that the two different scaling curves, found for the bound-free and bound-bound transition, do coincide. In these papers, we considered a model where all particles were treated as scalars [40], and a model where only the quarks were treated as scalars, while electrons and photons had their proper spin [41]. The treatment of the quarks as scalars considerably simplified our calculations, as the resulting Klein-Gordon equation could be solved analytically, by recognizing that it could be rewritten to resemble a Schrödinger equation. Once we introduced the proper spin for quarks [42,43], we solved the Dirac equation numerically, using a Runge-Kutta-Fehlberg (RKF) algorithm [50]. The numerical accuracy we achieved this way restricted us to momentum transfers below $q < 12$ GeV, a value where the calculated response functions had not fully converged to their scaling value yet. Even though we solved only for eigenenergies of up to 12 GeV, we found roughly 24 000 states below that energy. As for any relativistic problem, the density of energy states rapidly increases with the energy.

Thus, we could not determine if the bound-bound and bound-free scaling curves were going to coincide, as for the other, simplified models we investigated previously.

In a recent series of papers by Paris *et al.* [33–35], similar models were considered, and solved numerically, and the result found there was a pronounced discrepancy between the bound-free and bound-bound transition. This led the authors to question the interpretation of the scaling curves extracted from deep inelastic scattering (DIS). In DIS, it is generally assumed that final state interactions are negligible, and that the scaling curves can be interpreted in terms of parton distribution functions.

In this paper, we investigate the scaling behavior of our model with Dirac quarks. We do this by employing the

WKB method to solve the Dirac equation numerically for very high momentum transfers. This allows us to investigate the scaling behavior of the response functions in the bound-bound transition at the relevant high momentum transfers. The bound-free transition does not require any complicated final state calculations, and can be evaluated in a straightforward manner.

This paper is organized as follows: first, we remind the reader of the general ideas underlying the WKB approximation [51], and discuss the WKB for solving the Dirac equation. Then, we introduce our model and present numerical results obtained in the WKB approximation. We compare them to the results obtained by explicitly solving the differential equation at $q = 10$ GeV, the highest value accessible with the Runge-Kutta-Fehlberg method. After validating the WKB calculations, we proceed to investigate the scaling behavior of the bound-bound and bound-free transitions at large q , where convergence has set in.

II. THE WKB APPROXIMATION FOR THE DIRAC EQUATION

The Dirac Hamiltonian for a particle in a scalar field $S(r)$ and a timelike vector field $V(r)$ is

$$\hat{H} = \boldsymbol{\alpha} \cdot \hat{\mathbf{p}} + \beta(m + S(r)) + V(r). \quad (1)$$

The wave functions for the Dirac Hamiltonian are

$$\psi_{nljm}(\mathbf{r}) = \begin{pmatrix} \frac{G_{nl}(r)}{r} \mathcal{Y}_{lj}^m(\Omega_r) \\ i \frac{F_{nl}(r)}{r} \mathcal{Y}_{lj}^m(\Omega_r) \end{pmatrix} \quad (2)$$

where the $\mathcal{Y}_{lj}^m(\Omega_r)$ are the usual spin spherical harmonics. Then angular momentum quantum numbers are $l = -(\kappa + 1)$ for $\kappa < 0$ and $l = \kappa$ for $\kappa > 0$ with $\bar{l} = -\kappa$ for $\kappa < 0$ and $\bar{l} = \kappa - 1$ for $\kappa > 0$. The reduced radial wave functions $G(r)$ and $F(r)$ are solutions to the coupled equations

$$\hbar G'(r) + \hbar \frac{\kappa}{r} G(r) = (m + S(r) - V(r) + E)F(r), \quad (3)$$

$$\hbar F'(r) - \hbar \frac{\kappa}{r} F(r) = (m + S(r) + V(r) - E)G(r). \quad (4)$$

The differential equation can be solved numerically, but above a certain energy, finding the numerical solution with a standard Runge-Kutta-Fehlberg method [50,52] becomes inaccurate. In the relativistic treatment of a potential, the energy eigenvalues of higher states lie closer and closer together. At some high enough energy, the separation between neighboring states becomes so small that some states may be missed with shooting methods. Also, one always has to calculate all states consecutively, instead of being able to calculate a state with certain, given quantum numbers. While an improved method for the integration of the differential equation may be applied, the situation lends

itself to the application of a semiclassical approximation, the WKB method [51].

In order to illustrate that the assumptions of the WKB approximation are perfectly reasonable, we show a plot of a one-dimensional harmonic oscillator potential in Fig. 1, together with the exact solution of the wave function for an energy $E = 26\hbar\omega$. One can see that the wave function oscillates in the classically allowed region, where $E > V$, and strongly resembles a plane wave there. Outside of the classically allowed region, the wave function is damped and goes to zero.

The WKB approximation can be applied when the potential has only a small variation over several wavelengths of the particle, as is the case in Fig. 1 near the origin. This feature makes it quite useful for studying the highly energetic excited states of a particle bound in a potential. The WKB approximation assumes that in the classically allowed regions, the wave function can be approximated by a plane wave with a position-dependent effective wave vector. As the potential is almost constant over a few wavelengths, the change of the wave vector is small compared with the value of the local wave vector.

The WKB approximation can then be viewed as an expansion in derivatives of the effective phase. In the case of a one-dimensional wave equation, this is equivalent to an expansion in \hbar and is, therefore, often referred to as the semiclassical or quasiclassical approximation. In the case of the radial equation for a three-dimensional Schrödinger wave equation, care must be taken to correctly treat the centrifugal barrier term that arises from the angular momentum operator acting on the angular functions. This term is also important for the solution of the corresponding classical problem, and needs to be included in the leading-order effective potential for the WKB approximation, even though it will involve powers of \hbar . The WKB

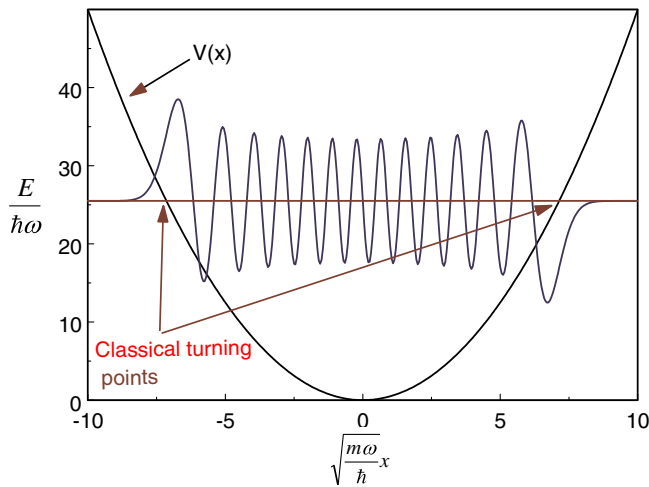


FIG. 1 (color online). The potential of a harmonic oscillator is shown, together with the exact wave function for an energy $E = 26\hbar\omega$.

approximation is then carried out by attaching an expansion parameter to the derivative terms in the wave equation and then proceeding as in the one-dimensional case.

To implement the WKB approximation for the Dirac equation the radial equations (3) and (4) are modified by making the substitution $\hbar\kappa \rightarrow \kappa$ and replacing the remaining factors of \hbar by the expansion parameter η to give

$$\eta G'(r) + \frac{\kappa}{r}G(r) = (m + S(r) - V(r) + E)F(r), \quad (5)$$

$$\eta F'(r) - \frac{\kappa}{r}F(r) = (m + S(r) + V(r) - E)G(r). \quad (6)$$

We now can parametrize the wave functions for positive energy solutions as

$$G(r) = e^{(i/\eta)\xi(r)} \quad (7)$$

and

$$F(r) = B(r)e^{(i/\eta)\xi(r)} \quad (8)$$

where $\xi(r)$ is the local phase for a plane wave and $B(r)$ allows for differences in the upper- and lower-component wave functions. Substituting these into (5) and (6) yields

$$i\xi'(r) + \frac{\kappa}{r} = (m + S(r) - V(r) + E)B(r), \quad (9)$$

$$\eta B'(r) + iB(r)\xi'(r) - \frac{\kappa}{r}B(r) = (m + S(r) + V(r) - E). \quad (10)$$

Equation (9) can be solved to give

$$B(r) = \frac{i\xi'(r) + \frac{\kappa}{r}}{m + S(r) + V(r) - E}. \quad (11)$$

Substituting (11) into (10) produces the second-order differential equation for the phase

$$i\eta\xi''(r) - \xi'(r)^2 - i\eta\frac{S'(r) - V'(r)}{m + S(r) - V(r) + E}\xi'(r) - \frac{\kappa^2}{r^2} - (m + S(r))^2 + (V(r) - E)^2 - \eta\frac{\kappa}{r}\left(\frac{1}{r} + \frac{S'(r) - V'(r)}{m + S(r) - V(r) + E}\right) = 0. \quad (12)$$

The WKB approximation is obtained by expanding the phase function in powers of η as

$$\xi(r) = \sum_{n=0}^{\infty} \eta^n \xi_n(r). \quad (13)$$

Substituting (13) into (12) gives

$$\begin{aligned}
& i \sum_{n=1}^{\infty} \eta^n \xi''_{n-1}(r) - \sum_{n=0}^{\infty} \eta^n \sum_{m=0}^n \xi'_m(r) \xi'_{n-m}(r) \\
& - \frac{S'(r) - V'(r)}{m + S(r) - V(r) + E} \sum_{n=1}^{\infty} \eta^n i \xi'_{n-1}(r) \\
& - \frac{\kappa^2}{r^2} - (m + S(r))^2 + (V(r) - E)^2 \\
& - \eta \frac{\kappa}{r} \left(\frac{1}{r} + \frac{S'(r) - V'(r)}{m + S(r) - V(r) + E} \right) = 0. \quad (14)
\end{aligned}$$

Equating coefficients of like powers of η gives

$$-\xi_0''(r) - \frac{\kappa^2}{r^2} - (m + S(r))^2 + (V(r) - E)^2 = 0 \quad (15)$$

for $n = 0$, and

$$\begin{aligned}
& i \xi_0''(r) - 2 \xi_0'(r) \xi_1'(r) - \frac{S'(r) - V'(r)}{m + S(r) - V(r) + E} i \xi_0'(r) \\
& - \frac{\kappa}{r} \left(\frac{1}{r} + \frac{S'(r) - V'(r)}{m + S(r) - V(r) + E} \right) = 0 \quad (16)
\end{aligned}$$

for $n = 1$.

Equation (15) can be solved to give

$$\xi_0'(r) = \pm \sqrt{(V(r) - E)^2 - (m + S(r))^2 - \frac{\kappa^2}{r^2}} \equiv \pm k_0(r) \quad (17)$$

and (16) can be solved to give

$$\begin{aligned}
\xi_1'(r) &= \frac{i}{2} \frac{\xi_0''(r)}{\xi_0'(r)} - \frac{i}{2} \frac{S'(r) - V'(r)}{m + S(r) - V(r) + E} - \frac{\kappa}{2 \xi_0'(r) r} \\
&\times \left(\frac{1}{r} + \frac{S'(r) - V'(r)}{m + S(r) - V(r) + E} \right) \\
&= i \Im(\xi_1'(r)) \pm k_1(r), \quad (18)
\end{aligned}$$

where

$$k_1(r) \equiv -\frac{1}{2k_0(r)} \frac{\kappa}{r} \left[\frac{1}{r} + \frac{S'(r) - V'(r)}{m + S(r) - V(r) + E} \right] \quad (19)$$

and

$$\begin{aligned}
\Im(\xi_1'(r)) &= \frac{1}{2} \frac{\xi_0''(r)}{\xi_0'(r)} - \frac{1}{2} \frac{S'(r) - V'(r)}{m + S(r) - V(r) + E} \\
&= \frac{d}{dr} \ln(\sqrt{k_0(r)}) - \frac{d}{dr} \\
&\times \ln(\sqrt{m + S(r) - V(r) + E}). \quad (20)
\end{aligned}$$

Keeping terms to order η , and using (17) and (18), the phase function can be integrated to give

$$\begin{aligned}
\xi(r) &= \int^r dr' (\xi_0'(r') + \eta \xi_1'(r')) \\
&= \int^r dr' \left[\pm k_0(r') + i \eta \frac{d}{dr'} \ln(\sqrt{k_0(r')}) - i \eta \frac{d}{dr'} \right. \\
&\quad \left. \times \ln(\sqrt{m + S(r') - V(r') + E}) \pm \eta k_1(r') \right] \\
&= i \eta \ln(\sqrt{k_0(r)}) - i \eta \ln(\sqrt{m + S(r) - V(r) + E}) \\
&\quad \pm \int^r dr' (k_0(r') + \eta k_1(r')). \quad (21)
\end{aligned}$$

The upper-component radial wave function can then be written as

$$\begin{aligned}
G(r) &= \mathcal{N} \frac{\sqrt{m + S(r) - V(r) + E}}{\sqrt{k_0(r)}} \\
&\times \exp \left[\pm \frac{i}{\eta} \int^r dr' (k_0(r') + \eta k_1(r')) \right], \quad (22)
\end{aligned}$$

where \mathcal{N} is the normalization constant.

The lower-component wave function can be obtained directly by using (11) to first order in η yielding

$$\begin{aligned}
F(r) &= \mathcal{N} \frac{1}{\sqrt{k_0(r)} \sqrt{m + S(r) - V(r) + E}} \\
&\times \left[\frac{\kappa}{r} - \eta \Im(\xi_1'(r)) \pm i(k_0(r) + \eta k_1(r)) \right] \\
&\times \exp \left[\frac{i}{\eta} \int^r dr' (k_0(r') + \eta k_1(r')) \right]. \quad (23)
\end{aligned}$$

From this point we will set $\eta = 1$ for convenience.

In constructing the above solution we have assumed that we are examining the solution in the classically allowed region where the energy E is greater than the effective potential. For the potentials which we will use, there is only one interval in r which is classically allowed. It is bounded by the classical turning points r_{\pm} which are the solutions to

$$k_0(r_{\pm}) = 0. \quad (24)$$

Quantization of the bound states is obtained by requiring that

$$\int_{r_-}^{r_+} dr' (k_0(r') + k_1(r')) = \left(n - \frac{1}{2} \right) \pi, \quad (25)$$

where $n \geq 1$, as in the Schrödinger case. The solutions can be extended to the classically forbidden regions by analytic continuation. Since the $k_0(r)$ vanishes at the classical turning points, the local wavelength $\lambda(r) = 2\pi/k_0(r)$ becomes arbitrarily large near the classical turning points in contradiction to the basic assumption of the WKB approximation. The expansion in η therefore does not converge in the vicinity of the classical turning points. Techniques for matching the wave functions at the turning points and replacing them with smooth approximate wave functions

near the turning points are well described in most introductory graduate quantum mechanics texts. There is, however, one additional complication in this case associated with the first-order phase $\xi_1(r)$ which does not appear in the Schrödinger case. This requires us to modify the usual approach to approximating the wave functions near the classical turning points. The solution to this complication is discussed in the Appendix.

We will need to construct the wave functions in three regions: the classically forbidden region where $0 \leq r < r_-$ (region I); the classically allowed region where $r_- \leq r \leq r_+$ (region II); and the classically forbidden region where $r_+ < r$ (region III). The wave functions must be matched at the boundaries. The procedure for the upper-component wave function is the same as for the Schrödinger case. Assume that we start by choosing the root in Eq. (17) where $\xi'_0(r) = +k_0(r)$. The wave function is then obtained by choosing

$$\mathcal{N} = \frac{N}{2} e^{-i(\pi/4)} \quad (26)$$

and then defining the wave function as

$$G_{\text{II}}(r) = G(r) + G^*(r). \quad (27)$$

This gives

$$G_{\text{II}}(r) = N \frac{\sqrt{m + S(r) - V(r) + E}}{\sqrt{k_0(r)}} \times \cos\left(\int_{r_-}^r dr' (k_0(r') + k_1(r')) - \frac{\pi}{4}\right). \quad (28)$$

Applying the same procedure to the lower component yields

$$F_{\text{II}}(r) = N \frac{1}{\sqrt{k_0(r)}\sqrt{m + S(r) - V(r) + E}} \left[\left(\frac{\kappa}{r} - \Im(\xi'_1(r)) \right) \times \cos\left(\int_{r_-}^r dr' (k_0(r') + k_1(r')) - \frac{\pi}{4}\right) \mp (k_0(r) + k_1(r)) \sin\left(\int_{r_-}^r dr' (k_0(r') + k_1(r')) - \frac{\pi}{4}\right) \right]. \quad (29)$$

In the classically forbidden regions the wave vectors become complex with

$$-ik_0(r) = \tilde{k}_0(r) = \sqrt{\frac{\kappa^2}{r^2} + (m + S(r))^2 - (V(r) - E)^2} \quad (30)$$

and

$$-ik_1(r) = \tilde{k}_1(r) = \frac{1}{2\tilde{k}_0(r)} \left[\frac{\kappa}{r^2} - \frac{\kappa}{r} \frac{S'(r) - V'(r)}{m + S(r) - V(r) + E} \right]. \quad (31)$$

The wave functions will be either growing exponentially or exponentially damped. Since we require that the wave functions be regular at the origin and damped at ∞ , we will construct the wave functions in the forbidden regions so that they fall off as r moves away from the turning points.

The solutions in region I require that the sign of the root $\tilde{\xi}'_0(r) = -\tilde{k}_0(r)$ be chosen so that the wave function vanishes at the origin. Choosing

$$\mathcal{N} = \frac{N}{2}, \quad (32)$$

the radial wave functions in this region are

$$G_I(r) = \frac{N}{2} \frac{\sqrt{m + S(r) - V(r) + E}}{\sqrt{\tilde{k}_0(r)}} \times \exp\left[-\int_r^{r_-} dr' (\tilde{k}_0(r') + \tilde{k}_1(r'))\right] \quad (33)$$

and

$$F_I(r) = \frac{N}{2} \frac{1}{\sqrt{\tilde{k}_0(r)}\sqrt{m + S(r) - V(r) + E}} \times \left(\frac{\kappa}{r} - \Im(\tilde{\xi}'_1(r)) + \tilde{k}_0(r) + \tilde{k}_1(r) \right) \times \exp\left[-\int_r^{r_-} dr' (\tilde{k}_0(r') + \tilde{k}_1(r'))\right]. \quad (34)$$

The solutions in region III are

$$G_{\text{III}}(r) = (-1)^{n-1} \frac{N}{2} \frac{\sqrt{m + S(r) - V(r) + E}}{\sqrt{\tilde{k}_0(r)}} \times \exp\left[-\int_{r_+}^r dr' (\tilde{k}_0(r') + \tilde{k}_1(r'))\right] \quad (35)$$

and

$$F_{\text{III}}(r) = (-1)^{n-1} \frac{N}{2} \frac{1}{\sqrt{\tilde{k}_0(r)}\sqrt{m + S(r) - V(r) + E}} \times \left(\frac{\kappa}{r} - \Im(\tilde{\xi}'_1(r)) - \tilde{k}_0(r) - \tilde{k}_1(r) \right) \times \exp\left[-\int_{r_+}^r dr' (\tilde{k}_0(r') + \tilde{k}_1(r'))\right]. \quad (36)$$

It should be pointed out that this is very similar to the WKB approximation to the Dirac equation described in [53–57]. In this previous work the WKB approximation is assumed to be in the form of a two-dimensional spinor of amplitude functions multiplied by the usual exponentiated phase function. Since the radial Dirac equations only determine two functions, it was necessary to make a choice for one of the amplitude functions that gives an upper-component wave function identical to that obtained here. The other two functions were obtained by solving two-

dimensional matrix equations by introducing a dual set of spinors for a non-Hermitian matrix and projecting to obtain scalar expressions for the phase function and the remaining amplitude function. However, this approach does not provide an expression for the first-order corrections to the phase that come from $\xi_1(r)$ in the derivation given here. These contributions are necessary for a simple, smooth extrapolation of the wave functions over the regions where the WKB approximation does not converge.

III. MODEL CALCULATIONS

Our model consists of a constituent quark bound to an infinitely heavy diquark and is represented by the Dirac Hamiltonian for a particle in a scalar field $S(r)$ and a timelike vector field $V(r)$.

$$\hat{H} = \boldsymbol{\alpha} \cdot \hat{\mathbf{p}} + \beta(m + S(r)) + V(r). \quad (37)$$

The scalar potential is a linear confining potential given by

$$S(r) = br, \quad b = 0.18013 \text{ GeV}^2. \quad (38)$$

In our model, the vector potential is provided by a vector color Coulomb potential. We will calculate for the case where the vector color Coulomb potential is absent, that is $V(r) = 0$, and where the vector potential is the simple static Coulomb potential

$$V(r) = -\frac{\beta}{r}, \quad (39)$$

with $\beta = 0.4$. For convenience, the mass has been chosen to be $m = 0$. For these potentials it is easily shown that the Dirac WKB wave functions have the correct functional dependence near $r = 0$ for all values of κ .

Note that we assume that the virtual photon only interacts with the light quark, and not with the infinitely heavy diquark. This still allows us to gain qualitative insight into the issues of scaling and duality, but makes a direct comparison of numerical results from our model to experimental data impossible: our model is much closer to electron scattering from a B meson than a proton. We would like to point out that therefore, the values obtained e.g. for the momentum transfer at the onset of scaling should not be compared to experimental values obtained in inclusive electron scattering from the proton. However, the question of whether the bound-bound and bound-free transitions lead to the same scaling curve can be discussed within this model.

One measure of the quality of the WKB approximation is a comparison of the eigenenergies calculated with the RKF method and the WKB approximation. Table I shows the eigenenergies for a few selected states. Since the WKB approximation should be most accurate at large energies and angular momenta, it is not surprising that the largest difference is for the ground state (lowest positive energy state), although even here the difference is less than 2 MeV. For the other states the difference is less than 0.1 MeV.

TABLE I. Comparison of eigenenergies calculated with RKF and WKB methods for a few selected states.

n	κ	E_{RKF} (GeV)	E_{WKB} (GeV)	$E_{\text{RKF}} - E_{\text{WKB}}$
1	-1	0.687 666	0.689 512	-0.001 84
60	5	6.697 930	6.697 904	0.000 026
196	-9	11.996 600	11.996 514	0.000 086
20	13	4.353 070	4.353 034	0.000 036
130	-22	10.051 700	10.051 677	0.000 023

Figure 2 shows the upper- and lower-component wave functions for $\beta = 0$ with $\kappa = -22$, $n = 130$, and $E = 10.051$ GeV (the last state listed in Table I). Wave functions are shown for both direct integration of the Dirac equation using the RKF method and for the WKB approximation. The range in r is chosen to cover the region of appreciable overlap between this state and the lowest positive energy state. The differences between the two sets of wave functions cannot be distinguished in this figure. This indicates that the Dirac WKB approximation is very good at these energies.

Figure 3 shows the longitudinal and transverse response functions for three-momentum transfers of $q = 10, 20$, and 30 GeV as a function of the y -scaling variable $y = \nu - q + E_{1,-1}$, where the response functions are related to the usual structure functions by

$$R_L(q, \nu) = \frac{q^4}{Q^4} W_2(Q^2, \nu) - \frac{q^2}{Q^2} W_1(Q^2, \nu) \quad (40)$$

and

$$R_T(q, \nu) = 2W_1(Q^2, \nu). \quad (41)$$

Each plot contains a comparison of the model with WKB wave functions to the response calculated assuming

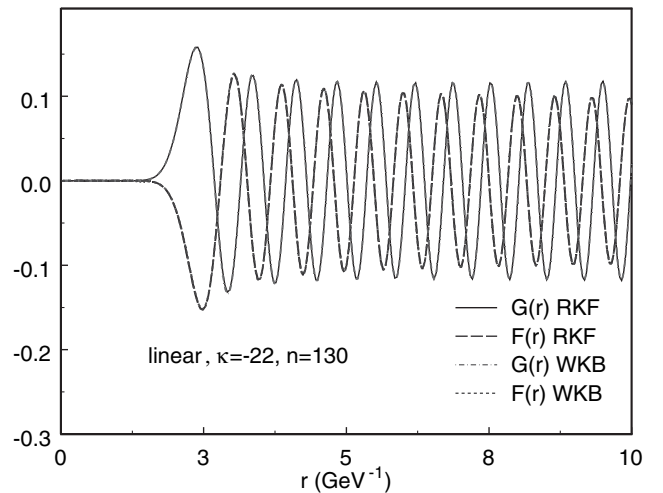


FIG. 2. Reduced radial wave functions for $\kappa = -22$ and $n = 130$ for a linear confining potential. Upper and lower components are shown for direct integration of the Dirac equation using the RKF method and in the WKB approximation.

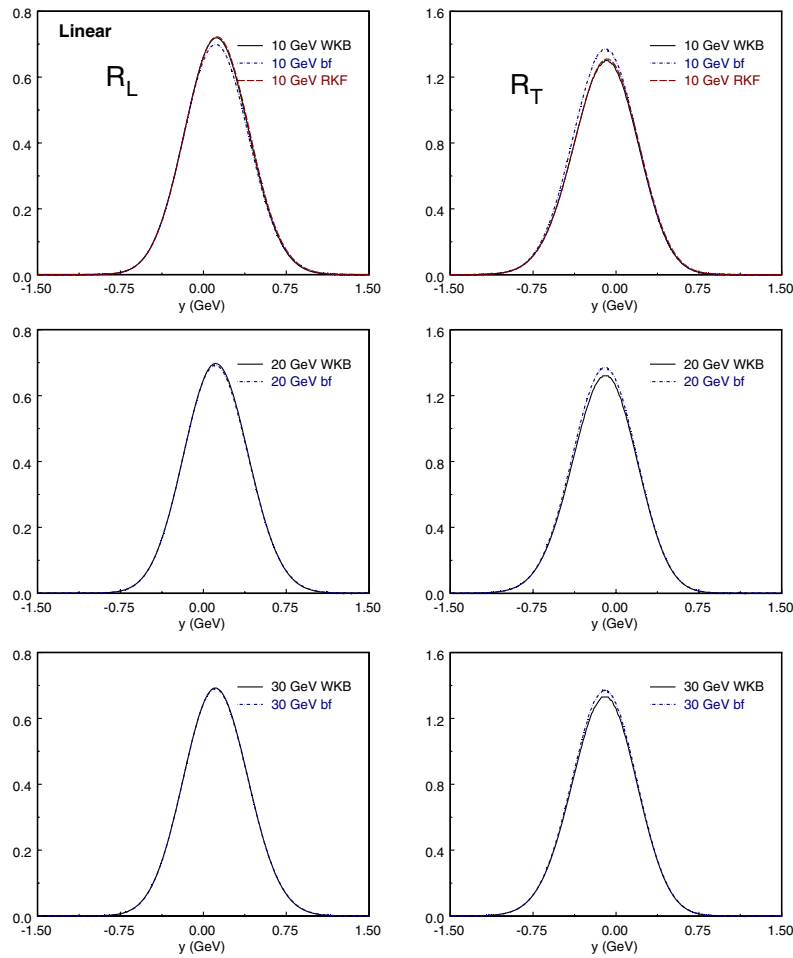


FIG. 3 (color online). Longitudinal and transverse response functions for the linear confining potential ($\beta = 0$) at $q = 10, 20,$ and 30 GeV. At each momentum transfer the bound-bound response function is compared to the bound-free response. The corresponding responses using the RKF integration are shown for comparison.

that the quark is ejected from the bound state to a plane-wave continuum state, the bound-free transition. This bound-free result is the model equivalent of the parton model. In addition, the plots for $q = 10$ GeV also show the model response calculated with RKF wave functions. It is clear from these that the RKF and WKB responses are virtually identical, as would be expected from the comparison of wave functions in Fig. 2. This figure shows that model response functions approach the corresponding bound-free response functions as the momentum transfer increases and that at $q = 30$ GeV they are almost identical. This indicates that the bound-bound transition within a model with a linear confining potential is dual to the bound-free case.

Figure 4 shows similar response functions for the case where the vector Coulomb potential is included. Again, the RKF and WKB response functions are very similar at $q = 10$ GeV. As the momentum transfer increases, the longitudinal model response for the bound-bound transition appears to be approaching the bound-free result from

above. For the transverse response, the bound-bound response is substantially smaller than the bound-free. Although the bound-bound response does slowly approach the bound-free with increasing momentum transfer, it is still quite far from the bound-free at $q = 30$ GeV. Also note that for both longitudinal and transverse responses the shapes of the model result and the bound-free results are slightly different and this does not seem to be changing with momentum transfer. This seems to indicate that the bound-bound and bound-free responses are not dual once the Coulomb potential is introduced. An extrapolation of the peak positions and values of the response functions has been performed fitting the bound-bound calculations at 10, 15, 20, 25, and 30 GeV to the form

$$R_{\max}(q) = A + \frac{B}{q} + \frac{C}{q^2}. \quad (42)$$

An estimate of the extrapolation error was obtained by varying the number of points in the fit from 3 to 5. Asymptotic values for the bound-free case are obtained

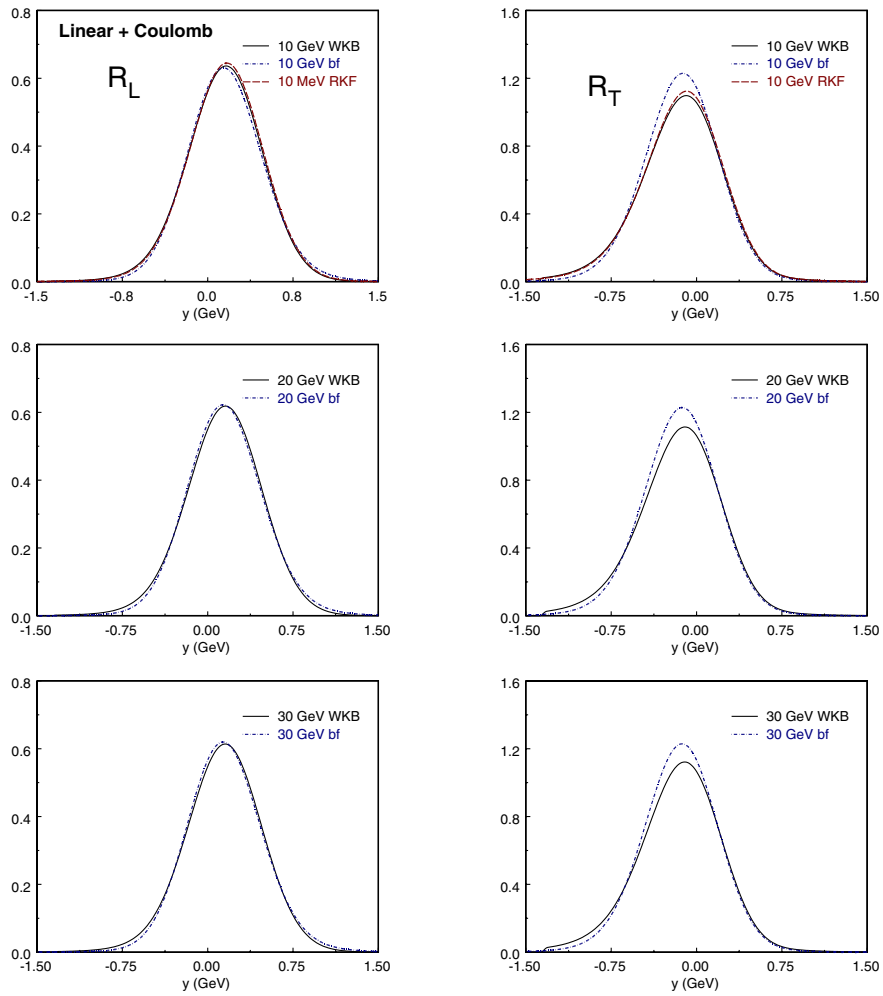


FIG. 4 (color online). Longitudinal and transverse response functions for the linear confining plus Coulomb potentials ($\beta = 0.4$) at $q = 10, 20,$ and 30 GeV. At each momentum transfer the bound-bound response function is compared to the bound-free (bf) response. The corresponding responses using the RKF integration are shown for comparison.

directly from a direct calculation of the responses in the limit $q \rightarrow \infty$. The results of the extrapolation are shown in Table II. For the case of the linear potential the positions and peak values of the bound-bound response functions do not vary significantly from the asymptotic bound-free response functions. However, for the linear-plus-Coulomb potential, there is a consistent shift in the peak position and the difference for the height of the transverse response is

substantial. A similar situation has been reported elsewhere for the case where the scalar and vector potentials are assumed to be identical linear confining potentials [34,35].

In this paper, we have presented a new method to solve the Dirac equation for scalar and timelike vector potentials in the WKB approximation. We have applied this method to calculating the response functions of a light quark bound to an infinitely heavy diquark in the bound-bound transi-

TABLE II. Extrapolation of the peak value R_{\max} and position y_{\max} of the peak of the response functions for $q \rightarrow \infty$. ΔR is the difference in peak height between the bound-free and bound-bound calculations.

		Bound-bound		Bound-free		ΔR
		y_{\max}	R_{\max}	y_{\max}	R_{\max}	
Linear	R_L	0.102	0.683 ± 0.005	0.105	0.685	0.002
	R_T	-0.106	1.358 ± 0.008	-0.105	1.370	0.012
linear + Coulomb	R_L	0.150	0.606 ± 0.003	0.132	0.614	0.008
	R_T	-0.108	1.137 ± 0.005	-0.132	1.229	0.092

tion at very high momentum transfers. This type of calculation is relevant for modeling quark-hadron duality. We compared these results to the bound-free transition, and found that the responses scale to the same limit for just a scalar potential. The vector potential introduces small differences in the two scaling functions.

ACKNOWLEDGMENTS

Two of the authors (S.J. and J.T.) thank the Theory Group of Jefferson Lab for their hospitality. This work was supported in part by funds provided by the U.S. Department of Energy (DOE) under cooperative research agreement No. DE-AC05-84ER40150 and by the National Science Foundation under Grant No. PHY-0139973 and No. PHY-0354916.

APPENDIX: THE DIRAC WKB WAVE FUNCTIONS NEAR THE TURNING POINTS

Since the WKB expansion does not converge near the classical turning points, the WKB wave functions near these points are not a good approximation to the exact wave functions and are, in fact, singular at the turning points. This problem can be eliminated by matching the WKB wave functions at some distance from the turning points to an exact or approximate solution to the wave equations near the turning points. The usual approach is to approximate the solution near the turning points by assuming that the potential is roughly linear over the region where the WKB wave functions fail. This gives matching conditions that lead to the phase factor in (26) and the corresponding wave functions are Airy functions $Ai(z)$. The matching to the WKB wave functions is achieved by using the limiting properties of the Airy function

$$\lim_{z \rightarrow \infty} \pi^{1/2} z^{1/4} Ai(z) \rightarrow \frac{1}{2} e^{-\zeta} \quad (\text{A1})$$

and

$$\lim_{z \rightarrow \infty} \pi^{1/2} z^{1/4} Ai(-z) \rightarrow \cos\left(\zeta - \frac{\pi}{4}\right), \quad (\text{A2})$$

where $\zeta = \frac{2}{3} z^{3/2}$ can be identified as the WKB phase function. The factors of $z^{1/4}$ cancel the singularity coming from the factor of $k_0^{-1/2}$ that appears in the definition of the WKB wave functions and gives a smooth finite result at the classical turning points.

A similar procedure can be used for the Dirac WKB wave functions once a few additional complications are dealt with. The primary problem is that the local wave vector $k_1(r)$ is singular at the turning points. This is a result of the factor of $k_0(r)$ that appears in (19). It is easy to show that near the turning points $k_0(r) \sim |r - r_{\pm}|^{1/2}$. Therefore, $k_1(r) \sim |r - r_{\pm}|^{-1/2}$. Since this singularity is integrable, $\Re \xi_1(r)$ will be finite at the turning points but will have infinite slope. This phase also changes sign at these points.

One result of this is to cause the total phase of the WKB wave functions to have an additional zero near the classical turning point. This interferes with the use of the usual Airy function approximation to the wave functions near the turning point for the upper-component wave function.

For the lower-component wave function, there is the additional complication that it contains an explicit factor of $k_1(r)$ and is therefore more singular at the turning point than can be canceled by the Airy function approximation, provided that a function that smoothly extrapolates to the sine function can be constructed. There is an additional problem arising from the factor of $k'_0(r)/k_0(r)$ that appears in (20). This behaves like $|r - r_{\pm}|^{-3/2}$ near the turning points and cannot be canceled by the Airy function solutions.

Consider the solution in region II given by (28). Define the phases

$$\zeta_i^I(r) = \int_r^{r_-} dr' \tilde{k}_i(r'), \quad (\text{A3})$$

$$\zeta_i^{\text{II}^-}(r) = \int_{r_-}^r dr' k_i(r'), \quad (\text{A4})$$

$$\zeta_i^{\text{II}^+}(r) = \int_r^{r_+} dr' k_i(r'), \quad (\text{A5})$$

$$\zeta_i^{\text{III}}(r) = \int_{r_+}^r dr' \tilde{k}_i(r'), \quad (\text{A6})$$

where $i = 0, 1$. Equation (28) can then be written as

$$\begin{aligned} G_{\text{II}}(r) &= N \frac{\sqrt{m + S(r) - V(r) + E}}{\sqrt{k_0(r)}} \\ &\quad \times \cos\left(\zeta_0^{\text{II}^-}(r) + \zeta_1^{\text{II}^-}(r) - \frac{\pi}{4}\right) \\ &= N \frac{\sqrt{m + S(r) - V(r) + E}}{\sqrt{k_0(r)}} \left(\cos\left(\zeta_0^{\text{II}^-}(r) - \frac{\pi}{4}\right) \right. \\ &\quad \left. \times \cos(\zeta_1^{\text{II}^-}(r)) - \sin\left(\zeta_0^{\text{II}^-}(r) - \frac{\pi}{4}\right) \sin(\zeta_1^{\text{II}^-}(r)) \right). \end{aligned} \quad (\text{A7})$$

Near the lower classical turning point, $\cos(\zeta_0^I(r) - \frac{\pi}{4})$ can be replaced by the Airy function using (A2) and $\sin(\zeta_0^I(r) - \frac{\pi}{4})$ can be replaced using the identity

$$\lim_{z \rightarrow \infty} \pi^{1/2} z^{-1/4} Ai'(-z) \rightarrow \sin\left(\zeta - \frac{\pi}{4}\right). \quad (\text{A8})$$

Therefore, near the lower classical turning point in region II we replace the WKB wave function (28) by

$$\begin{aligned}
 G_{II}(r) \rightarrow & N \frac{\sqrt{m + S(r) - V(r) + E}}{\sqrt{k_0(r)}} \pi^{1/2} [z(\zeta_0^{\Pi-}(r))]^{1/4} \\
 & \times \left(\text{Ai}(-z(\zeta_0^{\Pi-}(r))) \cos(\zeta_1^{\Pi-}(r)) \right. \\
 & \left. - \frac{1}{\sqrt{z(\zeta_0^{\Pi-}(r))}} \text{Ai}'(-z(\zeta_0^{\Pi-}(r))) \sin(\zeta_1^{\Pi-}(r)) \right). \quad (\text{A9})
 \end{aligned}$$

This can be continued across the lower turning point into region I using (A1) and the identity

$$-\lim_{z \rightarrow \infty} \pi^{1/2} z^{-1/4} \text{Ai}'(z) \rightarrow \frac{1}{2} e^{-\zeta} \quad (\text{A10})$$

to give

$$\begin{aligned}
 G_I(r) \rightarrow & N \frac{\sqrt{m + S(r) - V(r) + E}}{\sqrt{k_0(r)}} \pi^{1/2} [z(\zeta_0^I(r))]^{1/4} \\
 & \times \left(\text{Ai}(z(\zeta_0^I(r))) \cosh(\zeta_1^I(r)) \right. \\
 & \left. + \frac{1}{\sqrt{z(\zeta_0^I(r))}} \text{Ai}'(z(\zeta_0^I(r))) \sinh(\zeta_1^I(r)) \right). \quad (\text{A11})
 \end{aligned}$$

These wave functions are now continuous and smooth at the lower classical turning point, and match (28) and (33) away from the turning points. The solutions near the upper turning point are obtained by the replacement $\zeta_i^{\Pi-}(r) \rightarrow \zeta_i^{\Pi+}(r)$ in (A9) and for region III by the replacement $\zeta_i^I(r) \rightarrow \zeta_i^{\text{III}}(r)$ in (A11).

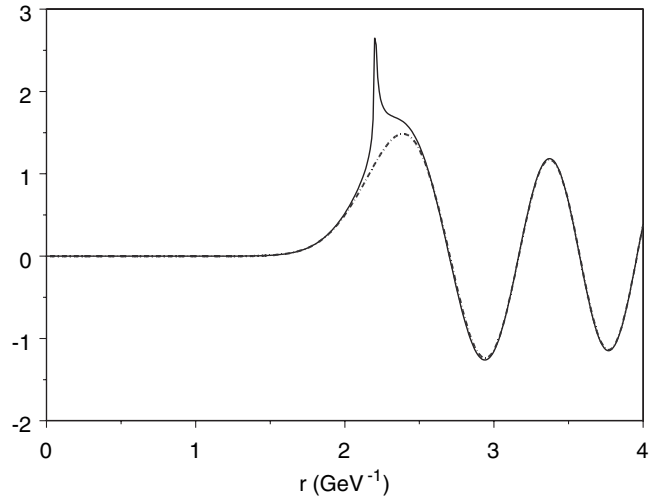


FIG. 5. The WKB wave function is shown as a solid line. The Airy function, which smoothly interpolates between the WKB wave functions in regions I and II, is shown as a dash-dotted line.

The corresponding expressions for the lower components can be obtained by using the expressions above in

$$F(r) = \frac{G'(r) + \frac{\kappa}{r} G(r)}{(m + S(r) - V(r) + E)}. \quad (\text{A12})$$

An example for the procedure outlined above is shown in Fig. 5. The solid line shows the WKB wave function given by (28) and (33), which clearly becomes singular at the turning point. The dash-dotted line is calculated using (A9) and (A11). The interpolation of the wave function using the Airy function clearly matches the WKB wave function within one wave length on either side of the classical turning point. Equations (28) and (33) can then be used to interpolate the WKB wave function through the region of the classical turning point where the WKB approximation is invalid.

- [1] E. D. Bloom and F. J. Gilman, Phys. Rev. Lett. **25**, 1140 (1970); Phys. Rev. D **4**, 2901 (1971).
- [2] R. F. Lebed and N. G. Uraltsev, Phys. Rev. D **62**, 094011 (2000).
- [3] See e.g. I. Bigi and N. Uraltsev, Int. J. Mod. Phys. A **16**, 5201 (2001); I. Bigi, M. Shifman, N. Uraltsev, and A. Vainshtein, Phys. Rev. D **59**, 054011 (1999); B. Grinstein and R. F. Lebed, Phys. Rev. D **59**, 054022 (1999); **57**, 1366 (1998); C. G. Boyd, B. Grinstein, and A. V. Manohar, Phys. Rev. D **54**, 2081 (1996).
- [4] N. Isgur and M. B. Wise, Phys. Rev. D **43**, 819 (1991).
- [5] See e.g. R. Rapp and J. Wambach, Adv. Nucl. Phys. **25**, 1 (2000).
- [6] M. A. Shifman, A. I. Vainshtein, and V. I. Zakharov, Nucl.

- Phys. **B147**, 448 (1979); M. A. Shifman, A. I. Vainshtein, and V. I. Zakharov, Nucl. Phys. **B147**, 385 (1979); A. I. Vainshtein, V. I. Zakharov, V. A. Novikov, and M. A. Shifman, Sov. J. Nucl. Phys. **32**, 840 (1980); E. C. Poggio, H. R. Quinn, and S. Weinberg, Phys. Rev. D **13**, 1958 (1976); A. V. Radyushkin, in *Strong Interactions at Low and Intermediate Energies*, edited by J. L. Goity (World Scientific, Singapore, 2000); T. D. Cohen, R. J. Furnstahl, D. K. Griegel, and X. Jin, Prog. Part. Nucl. Phys. **35**, 221 (1995).
- [7] I. Niculescu *et al.*, Phys. Rev. Lett. **85**, 1182 (2000); Phys. Rev. Lett. **85**, 1186 (2000); R. Ent, C. E. Keppel, and I. Niculescu, Phys. Rev. D **62**, 073008 (2000); S. Liuti, R. Ent, C. E. Keppel, and I. Niculescu, Phys. Rev. Lett. **89**,

- 162001 (2002).
- [8] Y. Liang *et al.* (Jefferson Lab Hall C E94-110 Collaboration), nucl-ex/0410027.
- [9] C.S. Armstrong, R. Ent, C.E. Keppel, S. Liuti, G. Niculescu, and I. Niculescu, Phys. Rev. D **63**, 094008 (2001).
- [10] J. Arrington, R. Ent, C.E. Keppel, J. Mammei, and I. Niculescu, nucl-ex/0307012; J. Arrington *et al.*, Phys. Rev. C **64**, 014602 (2001).
- [11] Z.E. Meziani *et al.*, Phys. Lett. B **613**, 148 (2005).
- [12] A. Airapetian *et al.* (HERMES Collaboration), Phys. Rev. Lett. **90**, 092002 (2003).
- [13] A. Fantoni (HERMES Collaboration), Eur. Phys. J. A **17**, 385 (2003).
- [14] J.-P. Chen, S. Choi, and N. Liyanage, Jefferson Lab Report No. E01-012, 2001.
- [15] D. Drakoulakos *et al.* (Minerva Collaboration), hep-ex/0405002.
- [16] C.J. Horowitz, M.A. Perez-Garcia, and J. Piekarewicz, Phys. Rev. C **69**, 045804 (2004).
- [17] Vipuli Dharmawarda (private communication).
- [18] F.E. Close and Q. Zhao, Phys. Rev. D **66**, 054001 (2002).
- [19] M. Diehl, Phys. Rep. **388**, 41 (2003).
- [20] W. Melnitchouk, Phys. Rev. Lett. **86**, 35 (2001); **93**, 199901(E) (2004).
- [21] W. Melnitchouk, K. Tsushima, and A.W. Thomas, Eur. Phys. J. A **14**, 105 (2002); F.M. Steffens and K. Tsushima, Phys. Rev. D **70**, 094040 (2004); K. Tsushima, K. Saito, and F.M. Steffens, Phys. Lett. B **612**, 5 (2005).
- [22] H. Gao and L. Zhu, *Pion Photoproduction on the Nucleon*, AIP Conf. Proc. No. 747 (AIP, New York, 2005), p. 179.
- [23] “*The Science Driving the 12 GeV Upgrade of CEBAF*,” edited by L. Cardman, R. Ent, N. Isgur, J.-M. Laget, C. Leemann, C. Meyer, and Z.-E. Meziani, Jefferson Lab, White Paper, 2001 (unpublished).
- [24] W. Melnitchouk, R. Ent, and C. Keppel, Phys. Rep. **406**, 127 (2005).
- [25] F.E. Close and N. Isgur, Phys. Lett. B **509**, 81 (2001).
- [26] F.E. Close and W. Melnitchouk, Phys. Rev. C **68**, 035210 (2003).
- [27] Q. Zhao and F.E. Close, Phys. Rev. Lett. **91**, 022004 (2003); Q. Zhao and F.E. Close, Int. J. Mod. Phys. A **20**, 1910 (2005).
- [28] C.E. Carlson, hep-ph/0005169; A. Afanasev, C.E. Carlson, and C. Wahlquist, Phys. Rev. D **62**, 074011 (2000).
- [29] C.E. Carlson and N.C. Mukhopadhyay, Phys. Rev. D **58**, 094029 (1998); **47**, R1737 (1993); **41**, 2343 (1990).
- [30] Y.B. Dong and J. He, Nucl. Phys. **A720**, 174 (2003).
- [31] Y.B. Dong and M.F. Li, Phys. Rev. C **68**, 015207 (2003).
- [32] Y.B. Dong, Nucl. Phys. **A744**, 293 (2004); Y.B. Dong and J. Liu, Nucl. Phys. **A739**, 166 (2004); Y.B. Dong and Q.G. Feng, Commun. Theor. Phys. **39**, 675 (2003); Y.B. Dong and M.F. Li, Commun. Theor. Phys. **39**, 193 (2003).
- [33] M.W. Paris and V.R. Pandharipande, Phys. Lett. B **514**, 361 (2001); M.W. Paris, Eur. Phys. J. A **17**, 401 (2003); M.W. Paris and V.R. Pandharipande, Phys. Rev. C **65**, 035203 (2002).
- [34] M.W. Paris, Phys. Rev. C **68**, 025201 (2003).
- [35] V.R. Pandharipande, M.W. Paris, and I. Sick, Phys. Rev. C **71**, 022201 (2005); V.R. Pandharipande, M.W. Paris, and I. Sick, Eur. Phys. J. A **24**, Suppl. 1, 143 (2005).
- [36] R. Fiore, A. Flachi, L.L. Jenkovszky, A.I. Lengyel, and V.K. Magas, Eur. Phys. J. A **15**, 505 (2002); L. Jenkovszky, V.K. Magas, and E. Predazzi, Eur. Phys. J. A **12**, 361 (2001).
- [37] A. Le Yaouanc, D. Melikhov, V. Morenas, L. Oliver, O. Pene, and J.C. Raynal, Phys. Lett. B **488**, 153 (2000).
- [38] G. Ricco, M. Anghinolfi, M. Ripani, S. Simula, and M. Taiuti, Phys. Rev. C **57**, 356 (1998); S. Simula, Phys. Lett. B **481**, 14 (2000).
- [39] K. Matsui, T. Sato, and T.S. Lee, nucl-th/0504051.
- [40] N. Isgur, S. Jeschonnek, W. Melnitchouk, and J.W. Van Orden, Phys. Rev. D **64**, 054005 (2001).
- [41] S. Jeschonnek and J.W. Van Orden, Phys. Rev. D **65**, 094038 (2002).
- [42] S. Jeschonnek and J.W. Van Orden, Phys. Rev. D **69**, 054006 (2004).
- [43] S. Jeschonnek and J.W. Van Orden, Phys. Rev. D **71**, 054019 (2005).
- [44] J.W. Van Orden and S. Jeschonnek, Eur. Phys. J. A **17**, 391 (2003).
- [45] M.A. DeWitt and S. Jeschonnek, *Prepared for 17th Annual HUGS at CEBAF (HUGS 2002), Newport News, Virginia, 2002* (World Scientific, Singapore, 2004).
- [46] Z. Batiz and F. Gross, Phys. Rev. D **69**, 074006 (2004).
- [47] S. Liuti, Eur. Phys. J. A **17**, 397 (2003); N. Bianchi, A. Fantoni, and S. Liuti, Phys. Rev. D **69**, 014505 (2004).
- [48] V.V. Davidovsky and B.V. Struminsky, Yad. Fiz. **66**, 1368 (2003) [Phys. At. Nucl. **66**, 1328 (2003)]; V.V. Davidovsky and B.V. Struminsky, hep-ph/0205130.
- [49] R. Hofmann, Prog. Part. Nucl. Phys. **52**, 299 (2004); R. Hofmann, Nucl. Phys. **B623**, 301 (2002).
- [50] E. Fehlbeg, Computing **6**, 61 (1970).
- [51] H. Jeffreys, Proc. London Math. Soc. **23**, 428 (1923); G. Wentzel, Z. Phys. **38**, 518 (1926); H.A. Kramers, Z. Phys. **39**, 828 (1926); L. Brillouin, Comptes rendus **183**, 24 (1926); Straightforward descriptions of the WKB or JWKB approximation for the Schrödinger equation are contained in most graduate level quantum mechanics texts.
- [52] W.H. Press, S.A. Teukolsky, W.T. Vetterling, and B.P. Flannery, *Numerical Recipes* (Cambridge University Press, Cambridge, England, 1992), 2nd ed.
- [53] V.D. Mur and V.S. Popov, Sov. J. Nucl. Phys. **28**, 429 (1978).
- [54] V.S. Popov and V.D. Mur, Sov. Phys. JETP **49**, 218 (1979).
- [55] V.D. Mur, V.S. Popov, Yu. A. Simonov, and V.P. Yurov, JETP **78**, 1 (1994).
- [56] V.V. Rubish, V. Yu. Lazur, O.K. Reity, S. Chalupka, and M. Salak, Czech. J. Phys. **54**, 897 (2004).
- [57] V. Yu. Lazur, O.K. Reity, and V.V. Rubish, Theor. Math. Phys. (Engl. Transl.) **143**, 559 (2005).